Clinical Cancer Research

Epithelial-to-Mesenchymal Transition Antagonizes Response to Targeted Therapies in Lung Cancer by Suppressing BIM

Kyung-A Song[1], Matthew J. Niederst[2,3], Timothy L. Lochmann[1], Aaron N. Hata[2,3], Hidenori Kitai[4], Jungoh Ham[1], Konstantinos V. Floros[1], Mark A. Hicks[1], Haichuan Hu[2,3], Hillary E. Mulvey[2,3], Yotam Drier[2,3], Daniel A.R. Heisey[1], Mark T. Hughes[1], Neha U. Patel[1], Elizabeth L. Lockerman[2,3], Angel Garcia[2,3], Shawn Gillepsie[2,3], Hannah L. Archibald[2,3], Maria Gomez-Caraballo[2,3], Tara J. Nulton[1], Brad E. Windle[1], Zofia Piotrowska[2,3], Sinem E. Sahingur[5], Shirley M. Taylor[6], Mikhail Dozmorov[7], Lecia V. Sequist[2,3], Bradley Bernstein[2,3], Hiromichi Ebi[4], Jeffrey A. Engelman[2,3], and Anthony C. Faber[1]

Abstract

Purpose: Epithelial-to-mesenchymal transition (EMT) confers resistance to a number of targeted therapies and chemotherapies. However, it has been unclear why EMT promotes resistance, thereby impairing progress to overcome it.

Experimental Design: We have developed several models of EMT-mediated resistance to EGFR inhibitors (EGFRi) in *EGFR*-mutant lung cancers to evaluate a novel mechanism of EMT-mediated resistance.

Results: We observed that mesenchymal *EGFR*-mutant lung cancers are resistant to EGFRi-induced apoptosis via insufficient expression of BIM, preventing cell death despite potent suppression of oncogenic signaling following EGFRi treatment. Mechanistically, we observed that the EMT transcription factor ZEB1 inhibits BIM expression by binding directly to the BIM promoter and repressing transcription. Derepression of BIM expression by depletion of ZEB1 or treatment with the BH3 mimetic ABT-263 to enhance "free" cellular BIM levels both led to resensitization of mesenchymal *EGFR*-mutant cancers to EGFRi. This relationship between EMT and loss of BIM is not restricted to *EGFR*-mutant lung cancers, as it was also observed in *KRAS*-mutant lung cancers and large datasets, including different cancer subtypes.

Conclusions: Altogether, these data reveal a novel mechanistic link between EMT and resistance to lung cancer targeted therapies. *Clin Cancer Res; 24(1); 197–208. ©2017 AACR.*

Introduction

Epithelial-to-mesenchymal (EMT) transition, in the context of carcinogenesis, describes the process by which carcinomas lose their apical–basal polarity and intracellular junctions, the result of which is a cancer cell that is more capable of migration, invasion, and intravasation into the bloodstream (1). Molecularly, EMT is largely driven by a number of related zinc finger–binding transcription factors (TF), which act in concert to induce these phenotypes. The gene expression changes brought on by EMT include loss of type IV collagens, inhibition of E-cadherin, and upregulation of fibronectins and vimentin (reviewed in refs. 2, 3). These gene expression changes are mediated directly by the mesenchymal zinc finger–binding TFs zinc finger E-box binding homeobox 1 (ZEB1), ZEB2, Twist, and Snail. Outside of the metastatic process, EMT has also garnered significant attention for its importance in response/resistance to anticancer therapies.

In non–small cell lung cancer (NSCLC) patients with *EGFR* mutations, large clinical trials have demonstrated that treatment with EGFR inhibitors (EGFRi) improves progression-free survival (PFS) in patients compared with those treated with chemotherapy (4, 5). On the basis of these data, treatment with EGFRi is currently standard-of-care first-line treatment for the estimated 10% to 15% of NSCLC patients whose cancers harbor activating mutations in *EGFR*. Despite the activity of EGFRi in *EGFR*-mutant NSCLC across clinical trials (4, 5), two critical barriers significantly limit their overall benefit to patients. First, initial responses are not uniform among *EGFR*-mutant patients, with 30% to 40% of patients failing to receive a marked regression that meets RECIST level (defined as a 30% reduction in tumor volume) response (4). Second, for the remaining patients, clinical responses are limited due to the phenomenon of "acquired resistance," which describes the cancers' adaptation to EGFRi therapy and subsequent

[1]Philips Institute for Oral Health Research, VCU School of Dentistry and Massey Cancer Center, Richmond, Virginia. [2]Massachusetts General Hospital Cancer Center, Boston, Massachusetts. [3]Department of Medicine, Harvard Medical School, Boston, Massachusetts. [4]Division of Medical Oncology, Cancer Research Institute, Kanazawa University, Kanazawa, Japan. [5]Department of Periodontics, VCU School of Dentistry, Virginia Commonwealth University, Richmond, Virginia. [6]Department of Microbiology and Immunology, Massey Cancer Center, Richmond, Virginia. [7]Department of Biostatistics, Virginia Commonwealth University, Richmond, Virginia.

Note: Supplementary data for this article are available at Clinical Cancer Research Online (http://clincancerres.aacrjournals.org/).

K.-A. Song and M.J. Niederst contributed equally to this article.

Corresponding Authors: Anthony C. Faber, Virginia Commonwealth University, Perkinson Building, Room 4134, 1101 East Leigh Street, Richmond VA 23298. Phone: 804-828-0841; Fax: 804-828-0150; E-mail; acfaber@vcu.edu; and Jeffrey A. Engelman, Novartis Institutes for Biomedical Research, 250 Massachusetts Avenue, Cambridge, MA 02139; E-mail: jeffrey.engelman@novartis.com

doi: 10.1158/1078-0432.CCR-17-1577

Translational Relevance

We have discovered a novel EMT axis whereby the mesenchymal transcriptional factor ZEB1 binds to the promoter and inhibits the expression of proapoptotic BIM. The resulting low levels of BIM expression lead to decreased sensitivity of mesenchymal cancers to targeted therapies in lung cancer. These findings may have implications beyond lung cancer, as we uncovered a striking inverse relationship between EMT and BIM expression across different cancer subsets as well.

regrowth. We and others have found that *EGFR*-mutant NSCLCs that have an EMT phenotype are associated with resistance to EGFRi therapy, both in the upfront setting and in the acquired resistance setting (6–10). These findings have spurred new efforts to uncover the molecular mechanisms underlying this type of resistance treatment in hopes of finding new therapies for these patients. Most notably, both AXL and SRC family members have been reported to contribute to EMT-mediated resistance to EGFRi by maintaining activation of key downstream signals (3, 6, 8).

Apoptosis, an extensively conserved programmed cellular death process, is vital to the efficacy of cancer therapeutics. Indeed, low apoptosis underlies upfront resistance in several other targeted therapy paradigms (11–15), and deficiencies in apoptosis contribute to resistance to EGFRi in *EGFR*-mutant NSCLCs (16, 17). Poor apoptotic response has been reported in a number of studies to be caused by deficient expression of the proapoptotic gene BIM, particularly the functional (BH3-containing) form (12, 13, 18, 19; reviewed in ref. 16). Indeed, low expression of functional BIM transcripts was shown to confer upfront resistance to EGFRi retrospectively in our previous study that examined a series of *EGFR*-mutant patient specimens (18), and low BIM mRNA was a retrospective predictor of overall response rate, PFS, and overall survival (OS) in a large patient cohort in the EURTAC trial (20, 21).

Herein, we investigate the role and mechanism of EMT-mediated depressed apoptosis following EGFRi treatment in resistance in *EGFR*-mutant NSCLCs.

Materials and Methods

Cell lines

The *EGFR*-mutant cell lines HCC4006, NCI-H1975, and HCC827 have been extensively characterized in previous publications (18, 22). The H1975 R2 cell line has been described previously (9). All cell lines were cultured in RPMI1640 (Lonza) with 10% FBS plus 1% penicillin and streptomycin (Gibco). Mycoplasma testing is routinely done on all the cell lines (Lonza), and the latest tests were performed in August 2017. We performed cell line authentication testing by SNP and STR analysis. These cell lines have been acquired over 36 months. MGH cell lines were established *EGFR*-mutant cell lines derived from EGFR inhibitor–resistant patients as described previously (23). The *KRAS*-mutant cell lines used in this study were described in a previous study (24).

Drugs

Gefitinib, WZ4002, dacomitinib (PF-299804), navitoclax (ABT-263), and venetoclax (ABT-199) were from AbMole. A-1331852 was kindly provided by AbbVie. Doxycycline hydrochloride was from Thermo Fisher Scientific. 4-Hydroxytamoxifen (4-OHT) was purchased from Sigma-Aldrich.

Western blotting

Western blots were performed as described previously (25) using the Invitrogen Midi-gel Tris-BIS system.

Immunoprecipitation

The indicated cells were lysed in the same buffer as used for Western blotting experiments: 25 μL of protein A sepharose beads (GE Healthcare, Bio-Sciences) were added to cellular lysates, followed by 0.5 μg of BIM antibody (cat# 2933, Cell Signaling Technology) or, when indicated, rabbit IgG (# sc-2027, Santa Cruz Biotechnology). Samples were incubated with motion at 4°C overnight. Immunoprecipitated complexes were washed three times in the same lysis buffer, boiled, and run on a 4% to 12% Bis-Tris gel (Invitrogen). Equal amounts of extracts (5% of immunoprecipitated protein) were prepared in parallel and run on the same gel.

ER-*TWIST*, *pTREX BIM*, shRNA, and siRNA experiments

The ER-*TWIST* plasmid, which contains a fusion of the hormone-binding domain of the estrogen receptor to *TWIST* and is conditionally activated by the presence of 4-OHT, has been previously described (26). Short hairpin RNA (shRNA) designed against *ZEB1* in the pLKO.1 vector has been described previously (27). si*ZEB1* was from Cell Signaling Technology and Invitrogen. Scramble control (Sc) siRNA was from Qiagen. The shGFP plasmid was described previously (27). The shSC plasmid was from Sigma-Aldrich (pLKO.1). shRNA transduction methodology has been described previously (28). The total concentration of siRNA used in each experiment was 100 nmol/L, and the siRNA was prepared with Hiperfect (Qiagen) in Optimem (Invitrogen).

Apoptosis and cell-cycle determination

Apoptosis and cell-cycle determination were performed in triplicate on a Millipore Guava except for Fig. 4A, which was performed on an LSR II (BD Biosciences). Cells were stained with propidium iodide and Annexin conjugated to Cy5 (BioVision). Cells stained positive for Annexin were counted as apoptotic. For cell-cycle analysis, pelleted cells were gently lysed with 0.1% Triton X-100, and cells were stained with propidium iodide. DNA content was quantified by gating using the Incyte module on the Millipore Guava.

qRT-PCR

ZEB1, *TWIST*, *BCL2L11* (BIM), and β-*actin* mRNA levels were determined by amplification and quantification of Sybr Green as described previously (29). The primer sequences are as follows: (i) *ZEB1* (F) 5′-gcacctgaagaggaccagag-3′, (R) 5′-tgcatctggtgttccatttt-3′; (ii) *TWIST* (F) 5′-ggagtccgcagtcttacgag-3′, (R) 5′-tctggaggacctggtagagg-3′; (iii) *BCL2L11* (F) 5′-atctcagtgcaatggcttcg-3′, (R) 5′-caactcttgggcgatccata-3′; (iv) β-*Actin* (F) 5′-agagctacgagctgcctgac-3′, (R) 5′-agcactgtgttggcgtacag-3′.

ZEB1 CRISPR/Cas9

The ZEB1 guide RNAs were from the GenCRISPR construct service (GenScript). The empty lentiCRISPR v2 was a gift from Feng Zhang; Addgene plasmid #52961 (30).

Animal experiments

We injected H1975 ER-*TWIST* cells that had been in culture with 4-OHT, subcutaneously into the right flanks of randomized, 6- to 8-week-old female Nod/SCID gamma (NSG) mice. Mice began receiving treatments when tumors reached approximately 100 to 150 mm^3. The tumor size was subsequently measured three times per week using a digital caliper, and tumors were calculated as length $\times$ width^2 $\times$ 0.52. Administration of 4-hydroxytamoxifen was by intraperitoneal injection, and the 4-hydroxytamoxifen was dissolved in corn oil with beads (final concentration of 2.5 mg/mouse/injection) and injected 5 days per week. WZ4002 was administered by oral gavage 25 mg per kg of body weight in 10% 1-methyl-2-pyrrolidinone: 90% PEG-400. Navitoclax was administered by oral gavage at 80 mg per kg of body weight in a mixture of 60% Phosal 50 PG, 30% PEG 400 and 10% ethanol. All drugs were administered 5 days per week. There were 4 to 6 mice per cohort. The animal experiment was approved by the Virginia Commonwealth University Institutional Animal Care and Use Committee (IACUC protocol# AD10001048).

Chromatin immunoprecipitation sequencing

Chromatin immunoprecipitation sequencing (ChIP-seq) was performed as described previously (31). In brief, 2×10^7 H1975 and H1975 R2 were fixed in 1% formaldehyde. Sonication was calibrated such that DNA was sheared to between 400 and 1,000 bp. ZEB1 was immunoprecipitated with an antibody from Cell Signaling Technology, clone number D80D3. ChIP DNA was used to generate sequencing libraries by end repair (End-It DNA Repair Kit, Epicentre), 3′ A base overhang addition via Klenow fragment (NEB), and ligation of barcoded sequencing adapters. Barcoded fragments were amplified via PCR. Libraries were sequenced as 40-bp paired-end reads on an Illumina NextSeq500 instrument. The GEO accession number for these studies is GSE106896.

ZEB1 ChIP

ChIP was performed as described previously (29). Briefly, cells were fixed for 15 minutes in RPMI1640 media containing 10% FBS and 1% formaldehyde and fixation quenched through addition of glycine (final concentration 0.125 mol/L). Fixed cells were lysed and chromatin sheared to a size of 100 to 500 bp. ChIP was performed using 5 μg of an anti-ZEB1 antibody (Santa Cruz Biotechnology, cat# sc-25388X). As a negative control, normal rabbit IgG (Cell Signaling Technology, cat# 2729S) was used. Input samples were generated by taking the supernatant of the normal rabbit IgG immunoprecipitation. Input and ChIP samples were subjected to qPCR in sextuplet using primers against an E-box near the transcription start site (TSS) of *BCL2L11* (forward: cgggaggctagggtaca, reverse: caggctcggacaggtaaag), or against an E-box near the 5′-end of exon 2 of *BCL2L11* (forward: ctaaccccggg-gaagtcagag, reverse: agggtacccccaaacaaaat).

ChIP-seq data analysis

Short reads were aligned to the hg19 genome assembly (National Center for Biotechnology Information Build 37) with Bowtie2 v4.1.2 software for the alignment of short DNA sequences (32). Data were analyzed and bound sites (from ChIP followed by deep sequencing) were identified with MACS v1.4.2 (Model-based Analysis for ChIP-Seq) software for peak discovery and next-generation sequencing analysis (33). Occupied sites were identified by searching for groups of tags positioned in a sliding window of 500 bp. Experimental samples were compared against the controls using a Poisson distribution as assigned by the MACS aligner. The threshold for the number of tags that generated an interacting site was determined for a false-discovery rate (FDR) of 0.001. Peaks were also required to have at least 4-fold more tags (normalized vs. total number) than the control samples. Visualization was performed with the IGV v2.3.81 tool.

Analysis of co-genes

Cell line gene expression obtained from the Cancer Cell Line Encyclopedia (CCLE) website ("Entrez_2012_9-29") were placed into a high BIM expressed group or a low BIM expressed group based on expression limits determined empirically. Cell lines with intermediate expression of BIM were not analyzed. The correlation between BIM expression and all other genes was determined by comparing expression of each gene between the two BIM expression groups using the *t* test. The FDRs were determined on the basis of correction for multiplicity using the Benjamini–Hochberg method.

BIM and EMT gene analyses

For the low BIM versus high BIM analysis in relation to EMT genes, the lowest 20% BIM-expressing cells were considered low BIM, with the rest considered medium and high BIM. The Garnett dataset was downloaded from Oncomine premium edition, which is $\log_2$ transformed and median centered (www.oncomine.com, January 2017, Thermo Fisher Scientific). The Huang and colleagues' dataset and the expO dataset were obtained from R2 genomics analysis and visualization platform.

Statistical analyses

For Fig. 1A, the FDRs were determined on the basis of correction for multiplicity using the Benjamini–Hochberg method. For Fig. 1B–D and Supplementary Fig. S1, samples were separated into two groups by the low (bottom 20%) versus med/high (remaining 80%) BIM expression. Mann–Whitney *U* tests were performed to compare low BIM and high BIM groups from the datasets ($P < 0.05$ was considered significant). For Fig. 1D, based on our hypothesis that low BIM was associated with high mesenchymal markers, we identified the difference in expression between the two sample populations using a one-tailed Mann–Whitney *U* test. The data presented in Supplementary Fig. S8B underwent linear regression analysis (GraphPad), and a *P* value was assigned. Student *t* tests were performed in the other figures, with $P < 0.05$ equaling significance.

Results

Mesenchymal cancers have low BIM levels

On the basis of our previous work highlighting the critical role of BIM in targeted therapy–induced apoptosis (13, 15, 18–21), we sought to identify potential modifiers of BIM expression to inform possible future therapeutic strategies. To this end, we interrogated the CCLE (34) to investigate gene expression data of approximately 19,000 genes in 857 solid tumor cancer cell lines. With this dataset, we performed an unbiased expression analysis (details in Materials and Methods) to determine the relationship of the expression of each gene with that of BIM. The EMT marker vimentin is the strongest associated gene among approximately 19,000, being highly inversely correlated with BIM (*BCL2L11*;

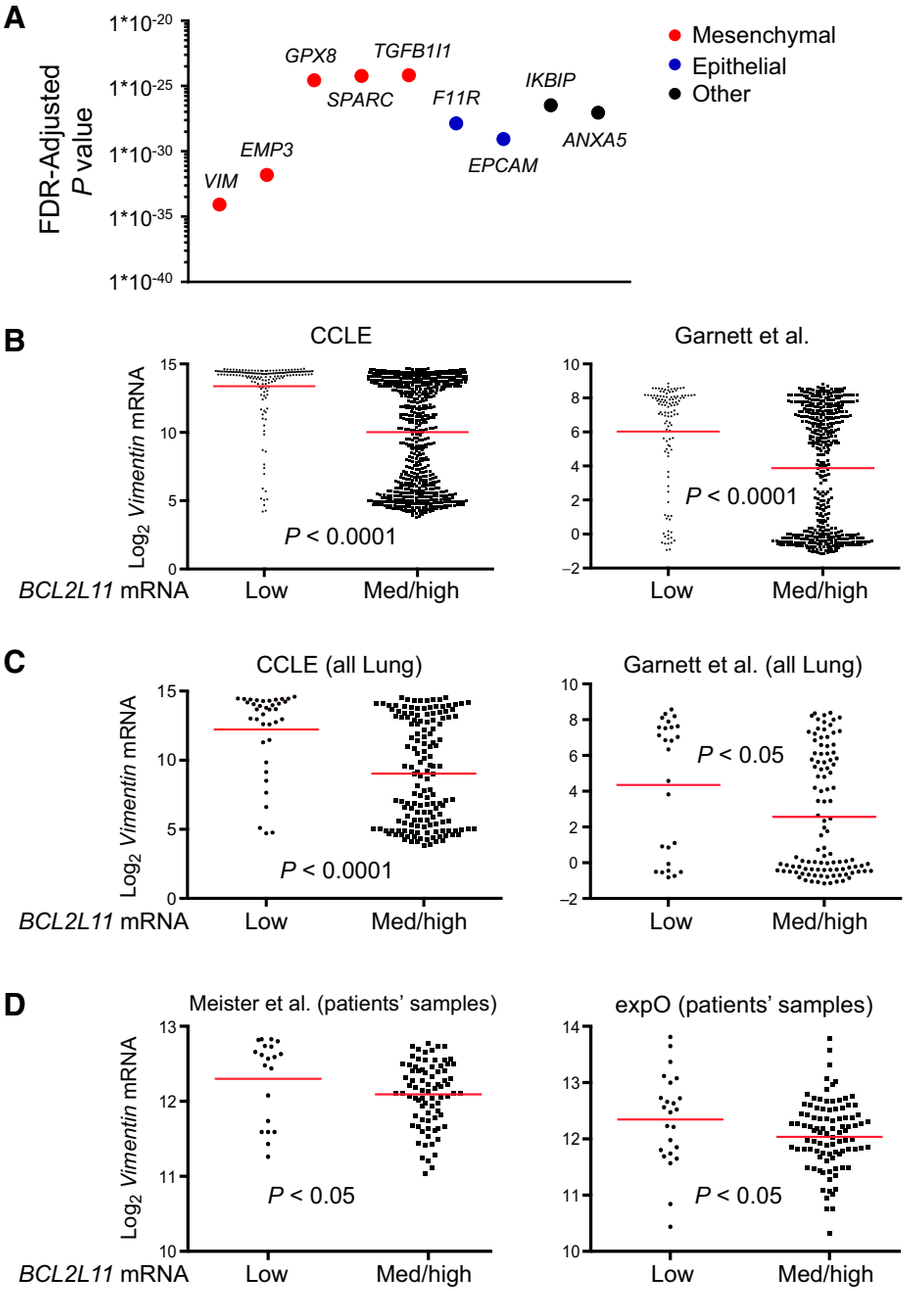

Figure 1.
Mesenchymal status and BIM (*BCL2L11*) levels are inversely correlated. **A,** Dot plot of the top nine genes correlated to BIM: known mesenchymal-related genes (red), epithelial-related genes (blue), or other genes (black) were plotted against *P* values. **B** and **C,** BIM mRNA levels were separated as low BIM and medium (med)/high BIM, and levels of the mesenchymal marker vimentin were plotted (each dot represents a unique solid tumor cancer cell line). **B,** Left, low $n = 171$, med/high $n = 686$; right, low $n = 114$, med/high $n = 459$. **C,** Left, low $n = 37$, med/high $n = 150$; right, low $n = 26$, med/high $n = 103$. Data were obtained from the CCLE (**B** and **C,** left) and Oncomine (**B** and **C,** right). **D,** BIM mRNA levels were separated as low BIM and medium (med)/high BIM, and levels of the mesenchymal marker vimentin were plotted (each dot represents a unique lung cancer patient sample). For both **D**, left panel (low $n = 20$, med/high $n = 80$), and **D**, right panel (low $n = 24$, med/high $n = 97$), the data were downloaded from the R2: Genomic Analysis and Visualization Platform. Please note that low BIM was considered the bottom 20% expressing cell lines and tumors.

$P = 8.69 \times 10^{-39}$; Supplementary Table S1). In addition, the expression of seven of the top nine correlated genes have been reported to be epithelial- or mesenchymal-related genes (Fig. 1A; Supplementary Fig. S1A and S1B; Supplementary Table S1). Although cancers with high BIM expression had a range of vimentin levels, those with low BIM expression almost uniformly had high vimentin expression (Fig. 1B, left).

We queried other deposited datasets in Oncomine (35), and a similar analysis of a second solid tumor cancer cell line database confirmed the striking relationship between mesenchymal cancers and low BIM expression (Fig. 1B, right). To determine whether mesenchymal cells had lower BIM expression specifically in lung cancers (encompassing both NSCLC and SCLC), we restricted the analysis to this cancer subtype. Again, we found low BIM to be strongly associated with mesenchymal status across both cell line datasets (Fig. 1C, left and right).

To test our hypothesis that low BIM associated with high vimentin expression in primary tumors, we identified a series of 80 NSCLC tumor samples from four primary locations, with 20 matched normal samples from the same patients (36) and confirmed the association between high vimentin expression and low expression of BIM (Fig. 1D, left). In addition, in a collection of 121 primary NSCLC tumors from the expression project for oncology (expO), we similarly found high vimentin expression associated

with low BIM expression (Fig. 1D, right). Altogether, these data demonstrate a strong relationship between low BIM expression and high mesenchymal gene expression.

To more directly test the impact of EMT on BIM expression and EGFRi efficacy, we induced EMT by utilizing an ER-*TWIST* plasmid that enables conditional activation of *TWIST* in the presence of 4-OHT (26). Following infection with ER-*TWIST*–containing virus and antibiotic resistance selection, we generated two *EGFR*-mutant NSCLC cell line derivatives that stably express the ER-*TWIST* construct (HCC4006 ER-*TWIST* and H1975 ER-*TWIST*). Subsequent treatment of these cells with 4-OHT induced an EMT, as evidenced by increased ZEB1 and decreased E-cadherin levels (Fig. 2A and B, left). Consistent with the correlative gene expression data in large cell line collections (Fig. 1), induction of an EMT in these cells was sufficient to promote a decrease in BIM_{EL} expression, the most abundantly expressed BH3-containing BIM isoform (37), both at the protein (Fig. 2A) and RNA level (Fig. 2B, right). Other key BCL-2 family antiapoptotic members were not markedly increased in the mesenchymal cells, with antiapoptotic MCL-1 levels lowered in the ER-*TWIST* cells treated with 4-OHT, which could be a result of loss of BIM-mediated stabilization of MCL-1 (Fig. 2A; ref. 38). Decreased BIM expression in the mesenchymal cells led to depressed apoptosis following EGFRi treatment (HCC4006; 1 μmol/L gefitinib, H1975; 1 μmol/L third-generation *EGFR*-mutant *L858R/T790M* inhibitor, WZ4002; Fig. 2C). Notably, this was despite similar shutdown of EGFR and downstream signaling pathways (Fig. 2D), leading to analogous growth arrest as evidenced by similar increases in the percent of cells in the G_1 phase of the cell cycle (Fig. 2E). Furthermore, WZ4002 treatment led to comparable increases in BIM protein in the parental and EMT cells, which is mediated by suppression of MEK/ERK (22, 37, 39), and decreases in MCL-1, which is mediated by suppression of PI3K/TORC1 (Fig. 2D; ref. 22). There were also increases in BIM mRNA levels in these cells, consistent with a contribution of BIM mRNA regulation by the MEK/ERK pathway (Supplementary Fig. S2A; ref. 40). Thus, depressed apoptosis was sufficient to result in the markedly poorer responses of the EMT cells to EGFRi in long-term viability assays (Fig. 2F; Supplementary Fig. S2B).

We next determined whether restoration of BIM in the cells induced to undergo an EMT was sufficient to resensitize to EGFRi. Titrating increasing amounts of BIM using a doxycycline-inducible system (18), we observed that increased BIM was sufficient to resensitize the EMT cancers to WZ4002 (Fig. 2G and H).

To further test the hypothesis that induction of EMT led to loss of BIM expression, we induced an EMT via a second approach; chronic exposure of *EGFR*-mutant cell lines to recombinant TGFβ (3). TGFβ-treated HCC827 cells (827T) underwent the expected characteristic changes attributed to EMT, including upregulation of ZEB1 and downregulation of E-cadherin (Supplementary Fig. S2C). In addition, the 827T cells had suppressed BIM protein and mRNA levels (Supplementary Fig. S2D) and were resistant to apoptosis induced by the EGFRi, gefitinib (Supplementary Fig. S2E). Furthermore, the PI3K and MEK/ERK pathways in the 827T cells remained sensitive to gefitinib, and the levels of the other BCL2 family members were not markedly affected by the EMT (Supplementary Fig. S2F). These findings are consistent with the ER-*TWIST* results (Fig. 2A and D) and are consistent with the hypothesis that diminished apoptosis was a result of the suppression of BIM. In a second *EGFR*-mutant cell line, chronic treatment with TGFβ similarly led to an EMT phenotype and reduced BIM levels (H1975T, Supplementary Fig. S2G and S2H), as well as a poorer apoptotic response to WZ4002 (Supplementary Fig. S2I). In summary, we believe that these results support the model that EMT induction suppresses BIM at the RNA level and mitigates EGFRi-mediated apoptosis.

BIM is suppressed in EGFRi-resistant models of *EGFR*-mutant NSCLC that undergo EMT

We found directly inducing EMT by exogenous *TWIST* activation (Fig. 2) or chronic TGFβ treatment (Supplementary Fig. S2) led to depressed levels of BIM, resulting in suppression of EGFRi-induced apoptosis and resistance to EGFRi (WZ4002 and gefitinib). We next sought to assess whether this mechanism of depressed BIM expression was similarly active in cells with acquired resistance to EGFRi. These resistant models were established as we have previously done by exposing sensitive cells to increasing amounts of EGFRi until they obtain the ability to survive and grow in the presence of EGFRi (9). The H1975 R1 and H1975 R2 cells (9) were developed by exposure to increasing concentrations of the pan-ErbB inhibitor/second-generation EGFR inhibitor PF-299804 (dacomitinib); these cells were cross-resistant to WZ4002 (Fig. 3A) and underwent an EMT (Fig. 3B). Consistent with the data from the induced EMT models (Fig. 2; Supplementary Fig. S2) and the gene expression data (Fig. 1; Supplementary Fig. S1), these cells had diminished levels of BIM at both the protein and RNA level (Fig. 3B and C). Two additional *EGFR*-mutant models that are sensitive to the third-generation EGFRi, WZ4002, the patient-derived treatment-naïve MGH119-1 (*exon 19 del*) and patient-derived erlotinib-resistant MGH164-2A (*exon 19 del/T790M*) cells, were made resistant to WZ4002 using the same approach as in the H1975 model (Supplementary Fig. S3, left). Multiple independent resistant lines with mesenchymal features were generated, and each line had suppressed BIM levels compared with the parental cells (Supplementary Fig. S3, right). These data indicate that in cell culture models of EMT-associated acquired resistance to EGFRi, BIM is likewise depressed.

ZEB1 directly binds to the BIM promoter and suppresses transcription in mesenchymal *EGFR*-mutant NSCLC cells

Low BIM RNA levels in mesenchymal cancers suggest that the regulation of BIM expression may be occurring at the transcriptional level (Figs. 1and 2B; Supplementary Figs. S1, S2A, S2D, and 2H). Therefore, we hypothesized that one of the number of well-characterized transcriptional repressors that is upregulated following EMT could be directly suppressing BIM transcription. Using the SwissRegulon portal (41), we searched for mesenchymal transcriptional regulators (6, 26) that had putative binding sites in the BIM promoter. From these analyses, we identified that the transcriptional repressor ZEB1 (2) was a candidate to bind the BIM promoter (Supplementary Fig. S4). It is noteworthy that vimentin had the highest positive gene correlation with ZEB1 among all other genes in 38 NSCLC cell lines (42) and, as would be expected, we found high ZEB1 was highly correlated with low BIM expression in the CCLE (Supplementary Fig. S5A). We next queried data archived in the ENCODE project of whole-genome ChIP-seq of ZEB1 in the HepG2 kidney cell line and identified ZEB1 binding in the BIM promoter (Fig. 3D). To determine the binding pattern of ZEB1 in the *EGFR*-mutant NSCLCs that underwent an EMT, we performed whole-genome ChIP-seq of ZEB1 in the mesenchymal H1975 R2 cells, as well as the epithelial H1975 parental cells for comparison. Analysis of ZEB1 enrichment

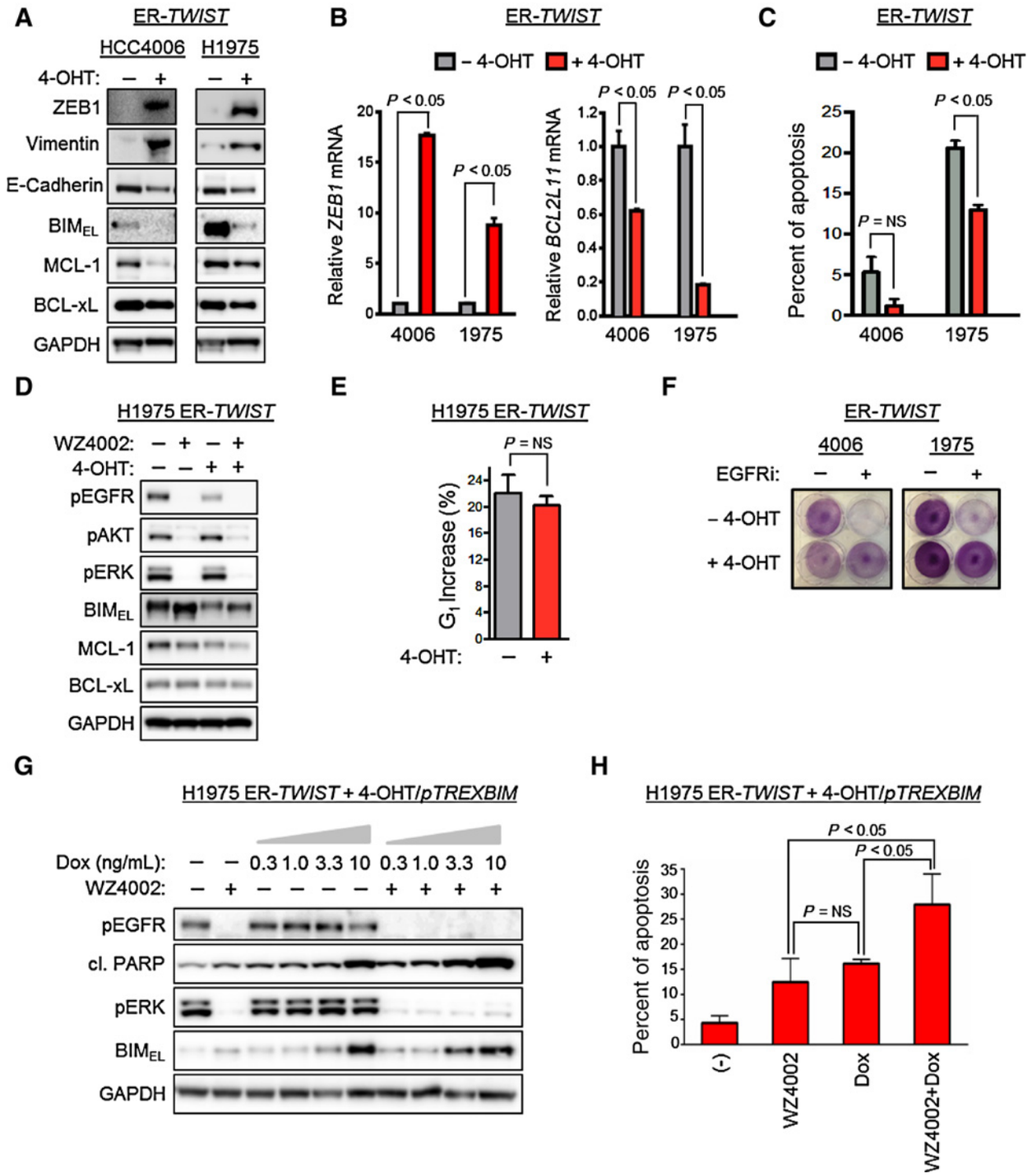

Figure 2.

EMT results in loss of BIM, loss of an apoptotic response to EGFR inhibitor, and loss of sensitivity to EGFR inhibitor. **A–C,** HCC4006 and H1975 *EGFR*-mutant NSCLC cell lines transduced with ER-*TWIST* were either conditionally activated with 4-OHT incubation (ER-*TWIST* + 4-OHT) or not (ER-*TWIST*), and lysates from the cells were probed with the indicated antibodies (**A**), RNA was isolated and relative ZEB1 (left) and BIM (*BCL2L11*) (right) levels determined by qPCR (**B**), or cells were treated with 1 μmol/L gefitinib (HCC4006) or 1 μmol/L WZ4002 (H1975) for 72 hours and apoptosis quantified (**C**). **D** and **E,** H1975 ER-*TWIST* and ER-*TWIST* + 4-OHT cells were treated with 1 μmol/L WZ4002 for 6 hours, and lysates were probed with the indicated antibodies (**D**) or treated for 24 hours, and cell G_1 cell-cycle increase was quantified by FACS (**E**). **F,** HCC4006 (4006) and H1975 (1975) ER-*TWIST* and ER-*TWIST* + 4-OHT cells were treated with 1 μmol/L gefitinib (4006) or 1 μmol/L WZ4002 (1975) for 5 days and cells stained with crystal violet. **G** and **H,** H1975 ER-*TWIST* + 4-OHT cells were further transduced with lentiviral particles containing a doxycycline-inducible BIM expression plasmid (*pTREXBIM*) and treated with 1 μmol/L WZ4002 with the indicated concentrations of doxycycline, and lysates were probed with the indicated antibodies (**G**) or apoptosis analysis was performed by FACS at 24 hours (**H**). Error bars, +SD for **B**, **E**, and **H**, and +SEM for **C**. **B**, **C**, and **H,** The indicated data points were repeated in triplicate, and the results are representative of three independent experiments. **E,** The indicated data points were repeated in triplicate, and the results are representative of two independent experiments.

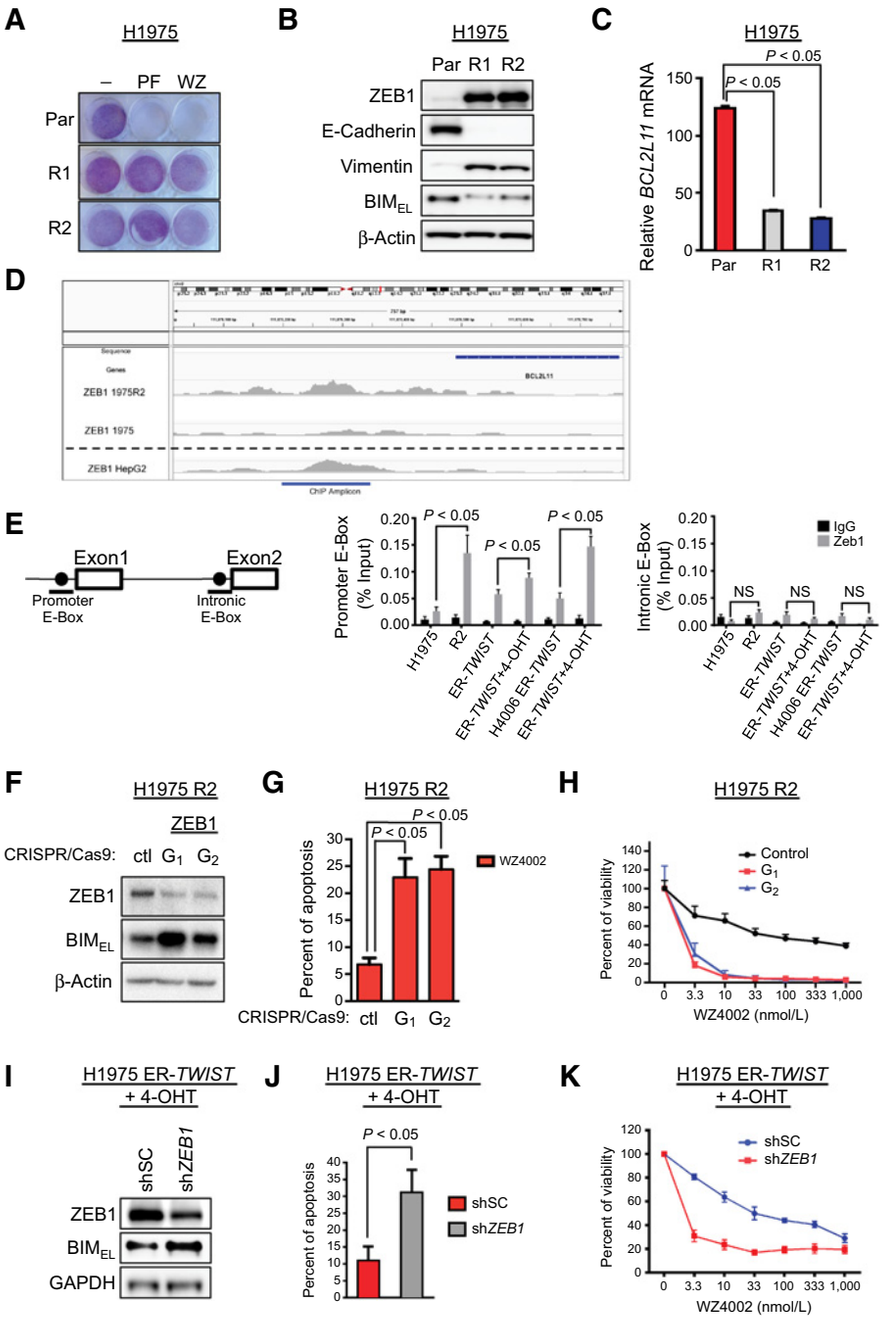

Figure 3.

ZEB1 directly binds and suppresses the BIM (*BCL2L11*) promoter to promote resistance to EGFR inhibition. **A–C,** Cells were treated with or without 1 μmol/L PF-299804 or 1 μmol/L WZ4002 for crystal violet staining (**A**), Western blotting (**B**), and RNA determination of H1975 parental cells (par), H1975 R1 cells (R1), and H1975 R2 cells (**C**; R2). **D,** ZEB1-binding profile within a 757-bp region encompassing the promoter and first exon of the BIM gene in wild-type ("ZEB1 1975") and mutated ("ZEB1 1975R2") cells. Density and pileup of sequencing reads are shown. The *y*-axes on both panels are equal scale. The "ZEB1 HepG2" panel shows ZEB1 binding in HepG2 cell line from ENCODE (separated by a dotted line to signify different source of data). **E,** ChIP of ZEB1 at the BIM promoter. ChIP was performed against ZEB1 (gray bars) or a nonspecific IgG antibody (black bars). Left, diagram of the first two exons of *BCL2L11*. E-box motifs, each 250 nt upstream of their respective exons, are denoted by a black circle. Quantification of amplicons is shown for each E-box for the (middle) residency of ZEB1 at the E-box immediately upstream of the *BCL2L11* transcriptional start site (promoter E-box) and (right) residency of ZEB1 at an E-box sequence immediately upstream of exon 2 of *BCL2L11* (intronic E-Box). The technical triplicates from duplicate qPCR run were used to determine the percent input of each amplicon. **F–H,** Transduction of virus containing ZEB1 CRISPR guide RNAs (CRISPR/Cas9, G1 and G2) in H1975 R2 cells followed by Western blotting (**F**), apoptosis induced by 1 μmol/L WZ4002 as measured by PI/Annexin staining and FACS (**G**), and 72-hour cell viability assay treated with the indicated doses of WZ4002 (**H**). **I–K,** Transduction of virus containing shSC or shZEB1 plasmids in H1975 ER-*TWIST* + 4-OHT cells followed by Western blotting (**I**), apoptosis induced by 1 μmol/L WZ4002 as measured by PI/Annexin staining and FACS (**J**), and 72-hour cell viability assay treated with the indicated doses of WZ4002 (**K**). Error bars, +SD for **C**, **H**, and **K**, and +SEM for **E**, **G**, and **J**. **C** and **G,** The indicated data points were repeated in triplicate, and the results are representative of three independent experiments. **J,** The indicated data points were repeated in triplicate, and the results are representative of three independent experiments. **H** and **K,** The indicated data points were repeated in quadruplicate, and the results are representative of two independent experiments.

profiles identified 9,744 unique peaks specific to the H1975 R2 cells that were not present in the H1975 parental cells. Evaluating a 1-Kb region upstream the transcription start site (TSS), we identified several classically repressed ZEB1 genes such as MUC-1 (43) and CRB3 (ref. 44; Supplementary Table S2). In addition, the BIM (*BCL2L11*) promoter was also directly bound by ZEB1, consistent with the data from our database analyses and cell culture experiments (Figs. 1–3; Supplementary Figs. S1–S3). Specifically, there was an enrichment peak in the H1975 R2 cells found approximately 200 bp upstream of the *BCL2L11* TSS, overlapping the previously identified ZEB1 binding location from HepG2 cells. These data suggest that ZEB1 binds to the *BCL2L11* promoter in H1975 R2 cells, leading to its transcriptional repression.

To validate the findings in our ChIP-seq studies, we performed follow-up ZEB1 ChIP studies in the H1975 ER-*TWIST* and HCC4006 ER-*TWIST* cell pairs. These experiments demonstrated similar binding of ZEB1 to the BIM promoter in the EMT cells as seen in the H1975 R2 cells, which was absent in the H1975 parental and the inactive ER-*TWIST* cells not treated with 4-OHT (Fig. 3E). These data demonstrate that ZEB1 is a novel regulator of BIM through direct binding of the BIM promoter in EMT NSCLC. In addition, this regulation occurs in *EGFR*-mutant NSCLCs that are resistant to EGFR inhibition and underwent an EMT.

To confirm a functional role for ZEB1 in suppressing BIM levels, we genetically depleted ZEB1 by short hairpin (sh) RNA or CRISPR in the H1975 R2 model. Consistent with the ChIP-seq and ChIP findings, knockdown of ZEB1 led to an increased expression of BIM, at both the protein and RNA level (Fig. 3F; Supplementary Fig. S5B; left and Supplementary Fig. S5C, left). Importantly, this depletion of ZEB1 also led to resensitization of H1975 R2 cells to WZ4002 (Fig. 3G and H; Supplementary Fig. S5C, middle and right). Similarly, in the H1975 EMT model induced by ER-*TWIST*, knockdown of ZEB1 led to derepression of BIM protein and RNA (Fig. 3I; Supplementary Fig. S5B, right) and restored EGFRi-induced apoptosis and resensitized these EMT cancers to WZ4002 (Fig. 3J and K). Furthermore, knockdown of ZEB1 with siRNA was also sufficient to derepress BIM in H1975 R2 (Supplementary Fig. S5D) and HCC4006 ER-*TWIST* cells (Supplementary Fig. S5E). These data demonstrate that ZEB1 suppresses BIM expression in cells that have undergone EMT, and depletion of ZEB1 restores BIM expression and sensitivity to EGFRi.

ABT-263 introduces an apoptotic response in mesenchymal *EGFR*-mutant lung cancers that have acquired resistance to EGFRi treatment

ZEB1 reduction leads to derepression of BIM in *EGFR*-mutant NSCLCs; however, ZEB1 is not as of yet directly druggable. We therefore sought a currently available pharmacologic solution to targeting EMT-mediated resistance in *EGFR*-mutant NSCLC. BH3 mimetics are effective anticancer drugs that work by reducing apoptotic thresholds through liberation of BIM from complexes with the prosurvival protein like BCL-2 and BCL-xL (27, 45). Furthermore, ABT-263 (navitoclax) is entering clinical trials with EGFRi in *EGFR*-mutant NSCLC (clinical trial number NCT02520778). We therefore tested whether treating the low BIM-expressing EGFRi-resistant mesenchymal H1975 R1 and H1975 R2 cells with ABT-263 would sufficiently increase free BIM levels to restore the apoptotic response to EGFRi. Indeed, the addition of ABT-263 to WZ4002 induced greater apoptosis in the resistant cells than that achieved by single-agent EGFRi in the parental cells (Fig. 4A). This translated to a marked sensitization to WZ4002 over 72 hours in proliferation assays (Fig. 4B). In the H1975 ER-*TWIST* model, the 4-OHT–treated cells likewise were sensitized to EGFRi with the addition of ABT-263 (Supplementary Fig. S6A). Interestingly, immunoprecipitation of BIM complexes in the H1975 R2 cells (Fig. 4C) or the H1975 ER-*TWIST* + 4-OHT cells (Supplementary Fig. S6B) demonstrated WZ4002 markedly increased the amount of BIM bound to (and therefore sequestered by) BCL-xL, but not BCL-2 or MCL-1. These data demonstrate how EGFR inhibition primes *EGFR*-mutant EMT cells for apoptosis, by BIM upregulation and MCL-1 downregulation, but this effect is mitigated by enhanced interaction with BCL-xL, which can be abrogated by ABT-263. As MCL-1 expression is a major resistance mechanism for ABT-263, EGFRi-mediated downregulation of MCL-1 likely contributes to the potency of the combination. Moreover, BCL-2/BIM complexes were not detectable (Fig. 4C, left; Supplementary Fig. S6B, left) despite BCL-2 expressed in the whole cell lysates (Fig. 4C, right; Supplementary Fig. S6B, right). Consistent with the notion this combination was effective through disruption of BCL-xL:BIM complexes, addition of the BCL-2 only inhibitor ABT-199 to WZ4002 only modestly increased apoptosis in the H1975 R2 cells, while the addition of a BCL-xL only inhibitor, A-1331852 (46), to WZ4002 led to similar levels of apoptosis as the WZ4002/ABT-263 combination (Supplementary Fig. S6C). Similarly, in two mesenchymal *EGFR*-mutant NSCLC lines that have poor apoptotic responses to WZ4002 alone (Supplementary Fig. S7A) and EGFRi-resistant mesenchymal models (Supplementary Fig. S7B), ABT-263 induced robust apoptosis that translated to dramatic reductions in long-term viability (Supplementary Fig. S7C). Finally, we tested the combination in an EMT mouse xenograft model. Mice bearing H1975 ER-*TWIST* tumors were treated intraperitoneally with 2.5 mg tamoxifen to induce an EMT [which we verified by Western blot analysis of the tumor lysate (Supplementary Fig. S8A)], and cohorts of mice were treated with WZ4002 (25 mg/kg), ABT-263 (80 mg/kg) or the combination at the same doses. Consistent with our *in vitro* observations, although single-agent WZ4002 was sufficient to markedly slow the growth of the tumors, the addition of ABT-263 was necessary to shrink tumors (Fig. 4D). Therefore, reestablishing an apoptotic response in EMT-mediated *EGFR*-mutant NSCLC-resistant cells is a promising pharmaceutical strategy.

ZEB1 regulates BIM in additional oncogene-addicted NSCLCs

The incidence of *EGFR*-activating mutations in NSCLC is usurped only by those in *KRAS*. To determine whether ZEB1 is also regulating BIM in *KRAS*-mutant mesenchymal NSCLCs, we interrogated five epithelial and five mesenchymal *KRAS*-mutant NSCLCs from a panel of *KRAS*-mutant lung cancer cell line models for ZEB1 and BIM expression. Western blotting revealed that 4 of 5 lowest BIM expressers were indeed mesenchymal like. As expected, these cancers expressed ZEB1 although the epithelial-like cancers did not (Fig. 4E). Consistently, within 39 *KRAS*-mutant NSCLC lines in CCLE, there was an inverse relationship between ZEB1 expression and BIM (Supplementary Fig. S8B). Furthermore, induction of an EMT in the H358 cells by chronic TGFβ treatment, led to repression of BIM, consistent with the effects of EMT on BIM expression in *EGFR*-mutant NSCLCs (Supplementary Fig. S8C). We knocked down ZEB1 expression

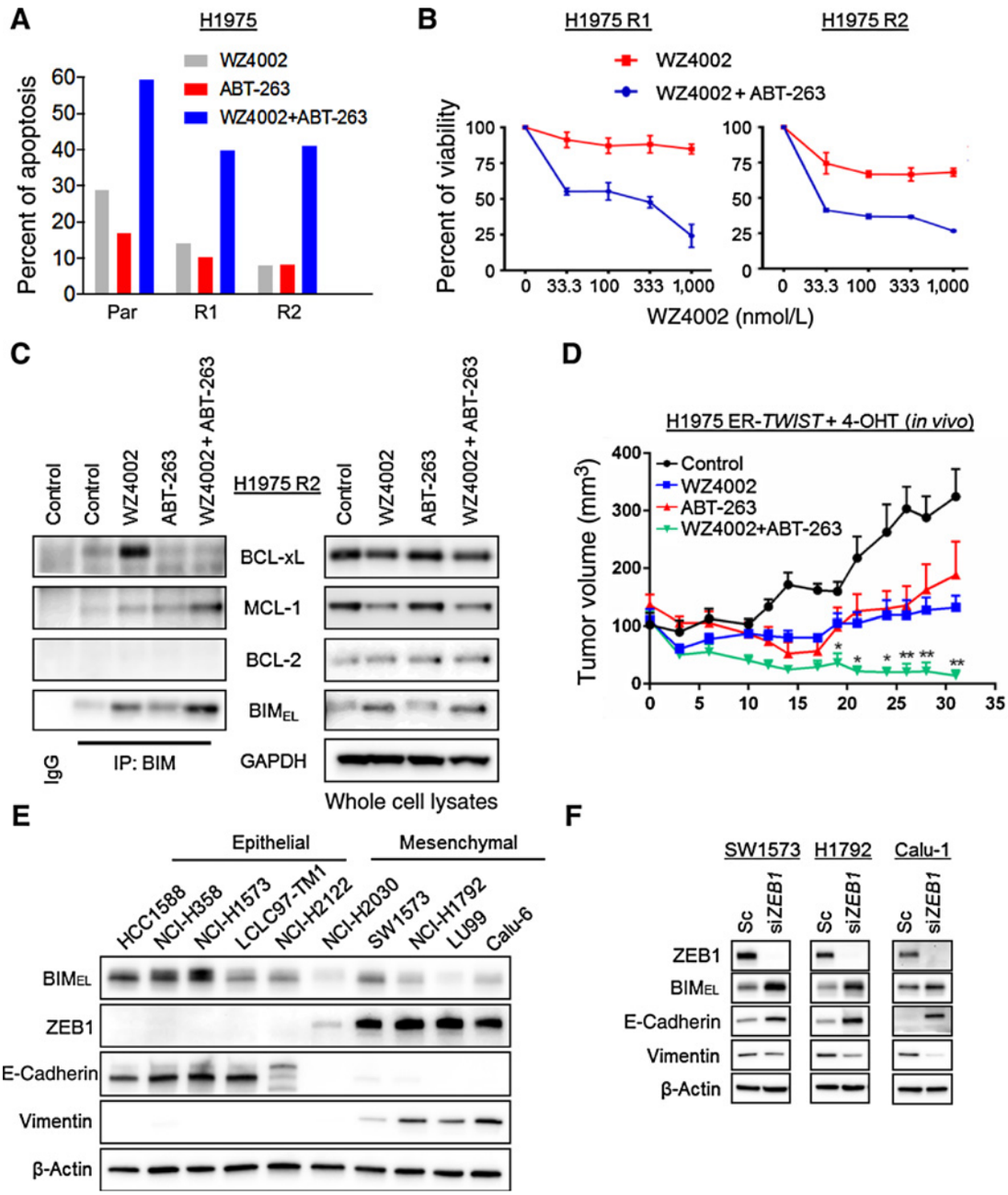

Figure 4.

Pharmacologic resensitization of EMT cells via ABT-263. **A** and **B,** Apoptosis measured by PI/Annexin staining and FACS following treatment with 1 μmol/L of the indicated drugs (**A**) and 72-hour cell viability assay with the indicated doses of WZ4002 ± 1 μmol/L ABT-263 of H1975 R1 cells and H1975 R2 cells (**B**). **C,** Western blots of BIM immunoprecipitation and whole-cell lysates of H1975 R2 cells. **D,** Mice harboring H1975 *ER-TWIST* + 4-OHT tumors were treated as indicated (**, $P < 0.01$; *, $P < 0.05$ compared with WZ4002). **E,** Five epithelial (left) and five mesenchymal (right) *KRAS*-mutant NSCLC cell lines were lysed and underwent Western blotting and probed with the indicated antibodies. **F,** *KRAS*-mutant NSCLCs were transfected with either a short-interfering (si) targeting a scramble (Sc) or ZEB1 sequence were lysed, and underwent Western blotting for the indicated antibodies. **B,** The indicated data points were repeated in quadruplicate, and the results are representative of two independent experiments.

in the mesenchymal SW1573, H1792, and Calu-1 cells and observed derepression of BIM in all three lines (Fig. 4F). Altogether, these data indicate that both *EGFR*- and *KRAS*-mutant NSCLCs that undergo EMT suppress BIM through ZEB1-mediated transcriptional repression, leading to targeted therapy resistance. The resistance in the mesenchymal cancers can be overcome by derepression of BIM via ZEB1 targeting or BCL2 family inhibition in combination with the appropriate targeted therapy.

Discussion

It has become increasingly clear that deficient apoptosis mitigates responses within a number of targeted therapy paradigms, including EGFRi in *EGFR*-mutant NSCLC (12–14, 18, 20). In addition, deficient BIM expression and EMT have independently associated with resistance to targeted therapies (3, 6, 8, 11, 13, 18–21, 47); however, to our knowledge, no link had been definitively established between the two.

In this study, we analyzed potential BIM modifiers and ultimately identified a novel ZEB1–BIM interaction that mediates low BIM expression in NSCLCs that undergo EMT, thereby revealing a mechanistic link between the two modes of resistance. ChIP-seq data reveal that the depression of BIM is mediated by direct ZEB1 binding to the BIM promoter and suppressing BIM transcription. Indeed, these data may also provide critical insights into EMT-associated resistance in multiple settings, as mesenchymal markers and low BIM expression are associated across multiple solid tumor types (Fig. 1A; Supplementary Figs. S1B and S5A), ZEB1 binds to the BIM promoter in non–lung cancer cells (Fig. 3D), and EMT is broadly associated with resistance to a number of targeted therapies, chemotherapies, and radiotherapy in various cancer types (10, 14, 28, 48–52).

EMT has been reported previously to specifically associate with resistance to EGFRi in *EGFR*-mutant and *EGFR* wild-type NSCLCs (6, 9, 26, 53–55). Src family kinases have been identified as potential mediators of resistance in mesenchymal cancers, although early-phase trials of NSCLC with the combination of gefitinib and the pan-Src inhibitor dasatinib did not support continuation of the combination. It should be noted these patients were molecularly unselected (56). Therefore, it remains an open question as to whether *EGFR*-mutant NSCLC patients with EMT would specifically derive benefit from this combination. EMT-mediated resistance has also been attributed to sustained activation of downstream signaling pathways by the AXL receptor tyrosine kinase (3, 6, 8). The role for AXL in mediating resistance also remains to be fully elucidated (47). More recently, NOTCH1 has been implicated in ZEB1-mediated EGFRi resistance in *EGFR*-mutant lung cancers (57). In our study, upon induction of EMT through conditional activation of *TWIST* or recombinant TGFβ treatment, there were no changes in either the ability of EGFR inhibitors to downregulate EGFR phosphorylation or downstream oncogenic signaling, namely the PI3K/AKT and MEK/ERK pathways. However, the ability of the EGFRi to induce apoptosis was markedly diminished. These data are consistent with a recent report, in which Settleman and colleagues treated *EGFR*-mutant HCC827 NSCLCs with recombinant TGFβ and saw marked differences in the ability of gefitinib to induce apoptosis, but not downregulate pEGFR, pAKT, or pERK (3). It has also long been appreciated that EMT confers apoptotic resistance to a number of anticancer therapeutics, including compounds not related to direct suppression of RTKs and downstream signaling pathways. Please note that low BIM is likely only one of multiple mechanisms whereby mesenchymal *EGFR*-mutant cancers are less sensitive to TKI. Our findings do support, however, that suppression of BIM is one meaningful mechanism by which the EMT program promotes targeted therapy resistance.

We recently reported that for the most prevalent resistant mechanism to EGFR inhibitors, namely acquisition of a secondary *T790M* mutation in *EGFR*, lung cancers can follow different paths to resistance: either development from a preexisting *T790M*-bearing clone or through *de novo* acquisition of *T790M* from drug-tolerant cells. Interestingly, in the drug-tolerant cell populations, as well as the fully resistant *T790M*-positive cells that emerged directly from them, analysis of RNA sequenicng data revealed an EMT signature, which was absent in both the parental cells and the resistant clones that emerged from preexisting *T790M*-positive cells (17). It is possible that the EMT cells in the population may survive the initial drug treatments due to apoptotic resistance, and, upon acquiring a means to reactivate the PI3K/MEK signaling pathways, for example via a *T790M* mutation, begin regrowth. This notion is further supported by our identification of patient-derived erlotinib-resistant cancer cell lines that are both mesenchymal and *T790M* positive (e.g., MGH721-1A). Taken together, these data are consistent with a model in which EMT-associated changes can potentially exert multiple protective effects on the cancer cell: (i) ZEB1 suppression of BIM protects the cell from drug-induced apoptosis and is important for maintaining initial survival and drug tolerance; and (ii) reactivation of downstream signaling via mechanisms that may include AXL/Src activity and/or the eventual acquisition of genetic alterations, such as *T790M* mutations, ultimately leading to reentry into the cell cycle and transition to a more complete resistant phenotype. Consistent with our observations of an important role of ZEB1-mediated survival of *EGFR*-mutant EMT cells, Larsen and colleagues have recently reported ZEB1 is the critical gene driving EMT in lung cancer (58).

Given the multiple findings that deficient functional BIM expression promotes EGFRi resistance, our findings further support implementation of therapeutic strategies that combine EGFRi with drugs that can overcome ZEB1-mediated suppression of BIM (13, 16, 18, 19). Indeed, we observed that acute depletion of ZEB1 was sufficient to derepress BIM and resensitize EMT cells to WZ4002 (Fig. 3F–K; Supplementary Fig. S5C). Although ZEB1 cannot be directly targeted at this time, this newly described mechanistic link between EMT and loss of BIM expression could be leveraged to identify therapeutic approaches to overcome EMT-induced resistance. For example, we observed that the reduced levels of BIM can potentially be overcome with direct targeting of BCL-xL as has been reported by others (13). The pharmaceutical approach of combining ABT-263 and an EGFRi could be successful in both *EGFR*-mutant lung cancers with EMT-mediated acquired resistance, as well as mesenchymal cancers in the upfront setting. In addition, our data suggest EMT marker expression could be used as a biomarker to direct patients that may benefit significantly from apoptotic derepression mediated by the combination of EGFRi and BH3 mimetics, which are entering the clinic for *EGFR*-mutant NSCLCs (i.e., clinical trial number NCT01009073). We have previously demonstrated that a combination of the third-generation EGFRi with ABT-263 can increase the amount of apoptosis (17) and importantly, in a previous small trial of 11 patients with different solid tumor malignancies, combining erlotinib and ABT-263 did not demonstrate new toxicities or significantly exacerbate single-drug toxicities, and, overall demonstrated tolerance (59). Finally, different targeted therapy paradigms, such as *BRAF*-mutant melanomas (15, 60) and *KRAS*-mutant cancers (27) that also have a clear rationale for use of targeted therapies in combination with ABT-263, EMT status may serve more broadly as a biomarker for these and other studies.

Overall, this study uncovers a molecular mechanism, ZEB1 suppression of BIM, which expands our understanding of the role

of apoptosis, and EMT in TKI resistance in *EGFR*-mutant NSCLCs. These findings should help inform future efforts to combat EMT-associated resistance in *EGFR*-mutant NSCLCs and may have more general implications for guiding therapeutic strategies in other EMT-associated resistant cancer paradigms.

Disclosure of Potential Conflicts of Interest

A.N. Hata reports receiving commercial research grants from Amgen, Novartis and Relay Therapeutics. Z. Piotrowska is a consultant/advisory board member for Ariad Pharmaceuticals, AstraZeneca, and Guardant Health. L.V. Sequist is a consultant/advisory board member for Ariad, AstraZeneca, Boehringer Ingelheim, Bristol-Myers Squibb, Clovis Oncology, Genentech, Merrimack, Novartis, and Pfizer. J.A. Engelman is an employee of and has ownership interests (including patents) at Novartis. No potential conflicts of interest were disclosed by the other authors.

Authors' Contributions

Conception and design: K.-A. Song, M.J. Niederst, K.V. Floros, B. Bernstein, J.A. Engelman, A.C. Faber

Development of methodology: M.J. Niederst, T.L. Lochmann, S.M. Taylor, A.C. Faber

Acquisition of data (provided animals, acquired and managed patients, provided facilities, etc.): M.J. Niederst, T.L. Lochmann, H. Kitai, J. Ham, M.A. Hicks, H. Hu, H.E. Mulvey, D.A.R. Heisey, M.T. Hughes, A. Garcia, S. Gillepsie, H.L. Archibald, Z. Piotrowska, L.V. Sequist

Analysis and interpretation of data (e.g., statistical analysis, biostatistics, computational analysis): K.-A. Song, M.J. Niederst, T.L. Lochmann, H. Kitai, K.V. Floros, H. Hu, Y. Drier, A. Garcia, T.J. Nulton, B.E. Windle, M. Dozmorov, H. Ebi, J.A. Engelman, A.C. Faber

Writing, review, and/or revision of the manuscript: K.-A. Song, M.J. Niederst, T.L. Lochmann, A.N. Hata, H. Hu, Y. Drier, M.T. Hughes, Z. Piotrowska, M. Dozmorov, L.V. Sequist, J.A. Engelman, A.C. Faber

Administrative, technical, or material support (i.e., reporting or organizing data, constructing databases): K.-A. Song, J. Ham, N.U. Patel, E.L. Lockerman, M. Gomez-Caraballo, S.E. Sahingur, H. Ebi, J.A. Engelman

Study supervision: A.C. Faber

Acknowledgments

A.C. Faber is supported by the George and Lavinia Blick Research Fund.

This work was supported by an American Lung Association Lung Cancer Discovery Award (to A.C. Faber), a NCIK22-CA175276 Career Development Award (to A.C. Faber), Uniting Against Lung Cancer (to M.J. Niederst), the Lung Cancer Research Foundation (to M.J. Niederst), a Department of Defense grant (to J.A. Engelman and L.V. Sequist), an American Cancer Society Institutional Grant (to A.C. Faber), a Grant-in-Aid from the Japan Agency for Medical Research and Development (Project for Cancer Research and Therapeutics Evolution; 16cm0106513h0001), a Grant-in-Aid for Scientific Research (KAKENHI 16K07164) to H. Ebi, and a National Institute of Dental and Craniofacial Research grant (DE025037) to S.E. Sahingur.

The costs of publication of this article were defrayed in part by the payment of page charges. This article must therefore be hereby marked *advertisement* in accordance with 18 U.S.C. Section 1734 solely to indicate this fact.

Received June 2, 2017; revised September 13, 2017; accepted October 13, 2017; published OnlineFirst October 19, 2017.

References

1. Tsai JH, Yang J. Epithelial-mesenchymal plasticity in carcinoma metastasis. Genes Dev 2013;27:2192–206.
2. Wang Y, Zhou BP. Epithelial-mesenchymal Transition—A Hallmark of Breast Cancer Metastasis. Cancer Hallm 2013;1:38–49.
3. Wilson C, Nicholes K, Bustos D, Lin E, Song Q, Stephan JP, et al. Overcoming EMT-associated resistance to anti-cancer drugs via Src/FAK pathway inhibition. Oncotarget 2014;5:7328–41.
4. Sequist LV, Martins RG, Spigel D, Grunberg SM, Spira A, Jänne PA, et al. First-line gefitinib in patients with advanced non-small-cell lung cancer harboring somatic EGFR mutations. J Clin Oncol 2008;26:2442–9.
5. Rosell R, Carcereny E, Gervais R, Vergnenegre A, Massuti B, Felip E, et al. Erlotinib versus standard chemotherapy as first-line treatment for European patients with advanced EGFR mutation-positive non-small-cell lung cancer (EURTAC): a multicentre, open-label, randomised phase 3 trial. Lancet Oncol 2012;13:239–46.
6. Byers LA, Diao L, Wang J, Saintigny P, Girard L, Peyton M, et al. An epithelial-mesenchymal transition gene signature predicts resistance to EGFR and PI3K inhibitors and identifies Axl as a therapeutic target for overcoming EGFR inhibitor resistance. Clin Cancer Res 2013;19:279–90.
7. Suda K, Tomizawa K, Fujii M, Murakami H, Osada H, Maehara Y, et al. Epithelial to mesenchymal transition in an epidermal growth factor receptor-mutant lung cancer cell line with acquired resistance to erlotinib. J Thorac Oncol 2011;6:1152–61.
8. Zhang Z, Lee JC, Lin L, Olivas V, Au V, LaFramboise T, et al. Activation of the AXL kinase causes resistance to EGFR-targeted therapy in lung cancer. Nat Genet 2012;44:852–60.
9. Sequist LV, Waltman BA, Dias-Santagata D, Digumarthy S, Turke AB, Fidias P, et al. Genotypic and histological evolution of lung cancers acquiring resistance to EGFR inhibitors. Sci Transl Med 2011;3:75ra26.
10. Chung JH, Rho JK, Xu X, Lee JS, Yoon HI, Lee CT, et al. Clinical and molecular evidences of epithelial to mesenchymal transition in acquired resistance to EGFR-TKIs. Lung Cancer 2011;73:176–82.
11. Hata AN, Yeo A, Faber AC, Lifshits E, Chen Z, Cheng KA, et al. Failure to induce apoptosis via BCL-2 family proteins underlies lack of efficacy of combined MEK and PI3K inhibitors for KRAS mutant lung cancers. Cancer Res 2014;74:3146–56.
12. Bean GR, Ganesan YT, Dong Y, Takeda S, Liu H, Chan PM, et al. PUMA and BIM are required for oncogene inactivation-induced apoptosis. Sci Signal 2013;6:ra20.
13. Ng KP, Hillmer AM, Chuah CT, Juan WC, Ko TK, Teo AS, et al. A common BIM deletion polymorphism mediates intrinsic resistance and inferior responses to tyrosine kinase inhibitors in cancer. Nat Med 2012;18:521–8.
14. Montero J, Sarosiek KA, DeAngelo JD, Maertens O, Ryan J, Ercan D, et al. Drug-induced death signaling strategy rapidly predicts cancer response to chemotherapy. Cell 2015;160:977–89.
15. Paraiso KH, Xiang Y, Rebecca VW, Abel EV, Chen YA, Munko AC, et al. PTEN loss confers BRAF inhibitor resistance to melanoma cells through the suppression of BIM expression. Cancer Res 2011;71:2750–60.
16. Hata AN, Engelman JA, Faber AC. The BCL2 family: key mediators of the apoptotic response to targeted anticancer therapeutics. Cancer Discov 2015;5:475–87.
17. Hata AN, Niederst MJ, Archibald HL, Gomez-Caraballo M, Siddiqui FM, Mulvey HE, et al. Tumor cells can follow distinct evolutionary paths to become resistant to epidermal growth factor receptor inhibition. Nat Med 2016;22:262–9.
18. Faber AC, Corcoran RB, Ebi H, Sequist LV, Waltman BA, Chung E, et al. BIM expression in treatment-naive cancers predicts responsiveness to kinase inhibitors. Cancer Discov 2011;1:352–65.
19. Nakagawa T, Takeuchi S, Yamada T, Ebi H, Sano T, Nanjo S, et al. EGFR-TKI resistance due to BIM polymorphism can be circumvented in combination with HDAC inhibition. Cancer Res 2013;73:2428–34.
20. Costa C, Molina MA, Drozdowskyj A, Giménez-Capitán A, Bertran-Alamillo J, Karachaliou N, et al. The impact of EGFR T790M mutations and BIM mRNA expression on outcome in patients with EGFR-mutant NSCLC treated with erlotinib or chemotherapy in the randomized phase III EURTAC trial. Clin Cancer Res 2014;20:2001–10.
21. Karachaliou N, Codony-Servat J, Teixidó C, Pilotto S, Drozdowskyj A, Codony-Servat C, et al. BIM and mTOR expression levels predict outcome to erlotinib in EGFR-mutant non-small-cell lung cancer. Sci Rep 2015;5:17499.

22. Faber AC, Li D, Song Y, Liang MC, Yeap BY, Bronson RT, et al. Differential induction of apoptosis in HER2 and EGFR addicted cancers following PI3K inhibition. Proc Natl Acad Sci U S A 2009;106:19503–8.
23. Crystal AS, Shaw AT, Sequist LV, Friboulet L, Niederst MJ, Lockerman EL, et al. Patient-derived models of acquired resistance can identify effective drug combinations for cancer. Science 2014;346:1480–6.
24. Kitai H, Ebi H, Tomida S, Floros KV, Kotani H, Adachi Y, et al. Epithelial-to-mesenchymal transition defines feedback activation of receptor tyrosine kinase signaling induced by MEK inhibition in KRAS-mutant lung cancer. Cancer Discov 2016;6:754–69.
25. Faber AC, Farago AF, Costa C, Dastur A, Gomez-Caraballo M, Robbins R, et al. Assessment of ABT-263 activity across a cancer cell line collection leads to a potent combination therapy for small-cell lung cancer. Proc Natl Acad Sci U S A 2015;112:E1288–96.
26. Salt MB, Bandyopadhyay S, McCormick F. Epithelial-to-mesenchymal transition rewires the molecular path to PI3K-dependent proliferation. Cancer Discov 2014;4:186–99.
27. Corcoran RB, Cheng KA, Hata AN, Faber AC, Ebi H, Coffee EM, et al. Synthetic lethal interaction of combined BCL-XL and MEK inhibition promotes tumor regressions in KRAS mutant cancer models. Cancer Cell 2013;23:121–8.
28. Ebi H, Corcoran RB, Singh A, Chen Z, Song Y, Lifshits E, et al. Receptor tyrosine kinases exert dominant control over PI3K signaling in human KRAS mutant colorectal cancers. J Clin Invest 2011;121:4311–21.
29. Ham J, Costa C, Sano R, Lochmann TL, Sennott EM, Patel NU, et al. Exploitation of the apoptosis-primed state of MYCN-amplified neuroblastoma to develop a potent and specific targeted therapy combination. Cancer Cell 2016;29:159–72.
30. Sanjana NE, Shalem O, Zhang F. Improved vectors and genome-wide libraries for CRISPR screening. Nat Methods 2014;11:783–4.
31. Ryan RJ, Drier Y, Whitton H, Cotton MJ, Kaur J, Issner R, et al. Detection of enhancer-associated rearrangements reveals mechanisms of oncogene dysregulation in B-cell lymphoma. Cancer Discov 2015;5:1058–71.
32. Langmead B, Trapnell C, Pop M, Salzberg SL. Ultrafast and memory-efficient alignment of short DNA sequences to the human genome. Genome Biol 2009;10:R25.
33. Zhang Y, Liu T, Meyer CA, Eeckhoute J, Johnson DS, Bernstein BE, et al. Model-based analysis of ChIP-Seq (MACS). Genome Biol 2008;9:R137.
34. Barretina J, Caponigro G, Stransky N, Venkatesan K, Margolin AA, Kim S, et al. The Cancer Cell Line Encyclopedia enables predictive modelling of anticancer drug sensitivity. Nature 2012;483:603–7.
35. Rhodes DR, Yu J, Shanker K, Deshpande N, Varambally R, Ghosh D, et al. ONCOMINE: a cancer microarray database and integrated data-mining platform. Neoplasia 2004;6:1–6.
36. Meister M, Belousov A, Xu EC, Schnabel P, Warth A, Hoffman H, et al. Intra-tumor heterogeneity of gene expression profiles in early stage non-small cell lung cancer. J Bioinform Res Stud 2014;1:1.
37. Ewings KE, Hadfield-Moorhouse K, Wiggins CM, Wickenden JA, Balmanno K, Gilley R, et al. ERK1/2-dependent phosphorylation of BimEL promotes its rapid dissociation from Mcl-1 and Bcl-xL. EMBO J 2007; 26:2856–67.
38. Czabotar PE, Lee EF, van Delft MF, Day CL, Smith BJ, Huang DC, et al. Structural insights into the degradation of Mcl-1 induced by BH3 domains. Proc Natl Acad Sci U S A 2007;104:6217–22.
39. Deng J, Shimamura T, Perera S, Carlson NE, Cai D, Shapiro GI, et al. Proapoptotic BH3-only BCL-2 family protein BIM connects death signaling from epidermal growth factor receptor inhibition to the mitochondrion. Cancer Res 2007;67:11867–75.
40. Meng J, Fang B, Liao Y, Chresta CM, Smith PD, Roth JA. Apoptosis induction by MEK inhibition in human lung cancer cells is mediated by Bim. PLoS One 2010;5:e13026.
41. SIB Swiss Institute of Bioinformatics Members. The SIB Swiss Institute of Bioinformatics' resources: focus on curated databases. Nucleic Acids Res 2016;44:D27–37.
42. Gemmill RM, Roche J, Potiron VA, Nasarre P, Mitas M, Coldren CD, et al. ZEB1-responsive genes in non-small cell lung cancer. Cancer Lett 2011;300:66–78.
43. Guaita S, Puig I, Franci C, Garrido M, Dominguez D, Batlle E, et al. Snail induction of epithelial to mesenchymal transition in tumor cells is accompanied by MUC1 repression and ZEB1 expression. J Biol Chem 2002; 277:39209–16.
44. Aigner K, Dampier B, Descovich L, Mikula M, Sultan A, Schreiber M, et al. The transcription factor ZEB1 (deltaEF1) promotes tumour cell dedifferentiation by repressing master regulators of epithelial polarity. Oncogene 2007;26:6979–88.
45. Faber AC, Coffee EM, Costa C, Dastur A, Ebi H, Hata AN, et al. mTOR inhibition specifically sensitizes colorectal cancers with KRAS or BRAF mutations to BCL-2/BCL-XL inhibition by suppressing MCL-1. Cancer Discov 2014;4:42–52.
46. Leverson JD, Phillips DC, Mitten MJ, Boghaert ER, Diaz D, Tahir SK, et al. Exploiting selective BCL-2 family inhibitors to dissect cell survival dependencies and define improved strategies for cancer therapy. Sci Transl Med 2015;7:279ra40.
47. Wilson C, Ye X, Pham T, Lin E, Chan S, McNamara E, et al. AXL inhibition sensitizes mesenchymal cancer cells to antimitotic drugs. Cancer Res 2014;74:5878–90.
48. Zhang P, Wei Y, Wang L, Debeb BG, Yuan Y, Zhang J, et al. ATM-mediated stabilization of ZEB1 promotes DNA damage response and radioresistance through CHK1. Nat Cell Biol 2014;16:864–75.
49. Arumugam T, Ramachandran V, Fournier KF, Wang H, Marquis L, Abbruzzese JL, et al. Epithelial to mesenchymal transition contributes to drug resistance in pancreatic cancer. Cancer Res 2009;69:5820–8.
50. Singh A, Settleman J. EMT, cancer stem cells and drug resistance: an emerging axis of evil in the war on cancer. Oncogene 2010;29:4741–51.
51. Siebzehnrubl FA, Silver DJ, Tugertimur B, Deleyrolle LP, Siebzehnrubl D, Sarkisian MR, et al. The ZEB1 pathway links glioblastoma initiation, invasion and chemoresistance. EMBO Mol Med 2013;5:1196–212.
52. Kim HR, Kim WS, Choi YJ, Choi CM, Rho JK, Lee JC. Epithelial-mesenchymal transition leads to crizotinib resistance in H2228 lung cancer cells with EML4-ALK translocation. Mol Oncol 2013;7:1093–102.
53. Witta SE, Gemmill RM, Hirsch FR, Coldren CD, Hedman K, Ravdel L, et al. Restoring E-cadherin expression increases sensitivity to epidermal growth factor receptor inhibitors in lung cancer cell lines. Cancer Res 2006;66: 944–50.
54. Xie M, He CS, Wei SH, Zhang L. Notch-1 contributes to epidermal growth factor receptor tyrosine kinase inhibitor acquired resistance in non-small cell lung cancer *in vitro* and *in vivo*. Eur J Cancer 2013;49:3559–72.
55. Thomson S, Petti F, Sujka-Kwok I, Epstein D, Haley JD. Kinase switching in mesenchymal-like non-small cell lung cancer lines contributes to EGFR inhibitor resistance through pathway redundancy. Clin Exp Metastasis 2008;25:843–54.
56. Gold KA, Lee JJ, Harun N, Tang X, Price J, Kawedia JD, et al. A phase I/II study combining erlotinib and dasatinib for non-small cell lung cancer. Oncologist 2014;19:1040–1.
57. Zhang T, Guo L, Creighton CJ, Lu Q, Gibbons DL, Yi ES, et al. A genetic cell context-dependent role for ZEB1 in lung cancer. Nat Commun 2016; 7:12231.
58. Larsen JE, Nathan V, Osborne JK, Farrow RK, Deb D, Sullivan JP, et al. ZEB1 drives epithelial-to-mesenchymal transition in lung cancer. J Clin Invest 2016;126:3219–35.
59. Tolcher AW, LoRusso P, Arzt J, Busman TA, Lian G, Rudersdorf NS, et al. Safety, efficacy, and pharmacokinetics of navitoclax (ABT-263) in combination with erlotinib in patients with advanced solid tumors. Cancer Chemother Pharmacol 2015;76:1025–32.
60. Frederick DT, Salas Fragomeni RA, Schalck A, Ferreiro-Neira I, Hoff T, Cooper ZA, et al. Clinical profiling of BCL-2 family members in the setting of BRAF inhibition offers a rationale for targeting de novo resistance using BH3 mimetics. PLoS One 2014;9:e101286.